

Magnetic field as a tracer for studying the differential rotation of the solar corona

O. G. Badalyan¹ · V. N. Obridko¹

© Springer ●●●

Abstract The characteristics of differential rotation of the solar corona for the period 1976–2004 were studied as a function of the distance from the center of the Sun. For this study, we developed a method using the coronal magnetic field as a tracer. The field in a spherical layer from the base of the corona up to the source surface was determined from photospheric measurements. Calculations were performed for 14 heliocentric distances from the base of the corona up to $2.45 R_{\odot}$ solar radii (the vicinity of the source surface) and from the equator to $\pm 75^{\circ}$ of latitude at 5° steps. For each day, we calculated three spherical components, which were then used to obtain the field strength. The coronal rotation periods were determined by the periodogram method. The rotation periods were calculated for all distances and latitudes under consideration. The results of these calculations make it possible to study the distribution of the rotation periods in the corona depending on distance, time, and phase of the cycle. The variations in the coronal differential rotation during the time interval 1976–2004 were as follows: the gradient of differential rotation decreased with the increase of heliocentric distance; the rotation remaining differential even in the vicinity of the source surface. The largest rotation rates (shortest rotation periods) were recorded at the cycle minimum at small heliospheric distances, *i.e.* small heights in the corona. The lowest rotation rate was observed at the middle of the ascending branch at large distances. At the minimum of the cycle, the differential rotation is most clearly pronounced, especially at small heliocentric distances. As the distance increases, the differential gradient decreases in all phases. The results based on magnetic data and on the brightness of the coronal green line 530.3 nm Fe XIV used earlier show a satisfactory agreement. Since the rotation of the magnetic field at the corresponding heights in the corona is probably determined by the conditions in the field generation region, an opportunity arises to use this method for diagnostics of differential rotation in the subphotospheric layers.

Keywords: Magnetic fields, Corona; Rotation

✉ V.N. Obridko
e-mail.obridko@izmiran.ru

O.G. Badalyan
e-mail.badalyan@izmiran.ru

¹ Pushkov Institute of Terrestrial Magnetism, Ionosphere, and Radio Wave Propagation, RAS, 108840, Troitsk, Moscow, Russia

1. Introduction

The present-day notion is that the rotation of the solar corona reflects the rotation of its subphotospheric layers. So, the differential rotation of the corona can provide us with additional information for the subsequent construction of solar dynamo models.

However, finding the coronal rotation parameters is not an easy task. In the corona, there are virtually no obvious tracers, such as, for example, sunspots or photospheric faculae, which help us study the rotation of the photosphere by tracing their position on the disk and calculating their speed, *i.e.*, the synodic rotation rate of the Sun. The Doppler method cannot be used because the coronal lines are too wide. Therefore, all existing studies of the differential rotation of the corona rely on the analysis of proxies, such as day-to-day changes in the brightness of the coronal emission lines or the features related to the corona (bright and dark areas, coronal holes, *etc.*).

Most studies are based on out-of-eclipse observations of the brightness of the coronal green line Fe XIV 530.0 nm above the limb. The list of such works is very extensive; we shall only mention some of them – Antonucci and Svalgaard (1974); Sýkora (1971a); Letfus and Sýkora (1982); Sime, Fisher, and Altrrock (1989); Makarov and Tlatov (1997); Rybák (1994, 2000); Altrrock (2003); Badalyan and Sýkora (2005, 2006); Badalyan, Obridko, and Sýkora (2006); Badalyan (2010). Some authors (*e.g.*, Tlatov, 1997; Altrrock, 2003) use also the red coronal line Fe X 673.4 nm. The possibility of conducting long-term extra-atmospheric observations made it possible to use typical coronal features as tracers. These are bright features (Zasatriet *al.*, 2009; Jurdana-Šepićet *al.*, 2011), dark features and $H\alpha$ filaments Brajša *et al.* (1997), 10.7 cm radio emission Mouradian, Bocchia, and Botton (2002), and coronal holes (Insley, Moore, and Harrison, 1995; Nash, Sheeley, and Wang, 1988). Most of these studies lead us to a general conclusion that the corona rotates differentially, the rotation parameters changing with the phase of the activity cycle.

Unfortunately, the tracers mentioned above characterize the rotation of the corona at relatively low heights above the limb. To study the rotation at significantly larger distances, we suggest using the fact that the structure of the corona up to a few solar radii is fully determined by the magnetic field. So far as direct magnetic measurements in the corona are impossible, the authors usually have to extrapolate the field measured in the photosphere. There are various methods for extrapolating observed photospheric magnetic fields to the coronal layers that are based on quite simple and physically consistent assumptions. Comparison with eclipse observations of the corona carried out by many authors shows a good agreement between the calculated and directly observed features. The agreement is also confirmed by theoretical comparison of the kinetic and magnetic pressure in the corona.

In this paper we use magnetic field calculations to study the rotation of the corona over a large range of distances from the center of the Sun – from the base of the corona to the source surface. In what follows, we mean by rotation of the corona (unless otherwise specified) the rotation of the calculated magnetic field. This method was proposed in Badalyan and Obridko (2015). It allows us

to trace changes in the differential rotation of the corona with distance and with the phase of the activity cycle and to compare them with the rotation parameters obtained from the study of other coronal tracers, *e.g.*, the brightness of the coronal green line.

This study covers the time interval from 24 June 1976 to 31 December 2004, i.e., Cycles 21, 22, and a part of Cycle 23. The magnetic field was calculated at selected distances from the base of the corona to the source surface. An important distance is $1.1 R_{\odot}$, which is close to the distance the coronal green-line brightness data we were using are reduced to (see Sýkora, 1971b, Storini and Sýkora, 1997, Sýkora and Rybák, 2005). The database covers the interval from 1939 to 2001, which allows us to compare the corona rotation parameters obtained from the green-line brightness and from the magnetic field at a given distance.

The main principles of our method for calculating the synodic rotation rate of the corona using the magnetic field as a tracer are described in Sections 2 and 3. Further, in Sections 4 and 5, we consider the variation in the rotation characteristics depending on the phase of the activity cycle and heliocentric distance. In Section 6, the results based on the magnetic data are compared with those obtained earlier from observations of the coronal green-line brightness. The Conclusion dwells on the possibility of using the results obtained to study the rotation characteristics of the subphotospheric layers of the Sun.

2. Method for calculating the magnetic field in the corona

We calculated the coronal magnetic field in the potential approximation using the well-known method described in Hoeksema and Scherrer (1986); Hoeksema (1991) in its classical version without assuming the radial field in the photosphere. We used as the source data WSO (John Wilcox Solar Observatory) measurements of the longitudinal component of the photospheric magnetic field (<http://wso.stanford.edu/synopticl.html>) and on their basis built the synoptic charts for each Carrington rotation. The general method for extrapolating the magnetic field in the corona is to solve the boundary problem with the line-of-sight field component measured in the photosphere and strictly radial field at the source surface. As a result, it becomes possible to calculate three magnetic field components in the spherical coordinates B_r , B_{θ} , B_{φ} .

The magnetic field components have the form:

$$B_r = \sum P_n^m(\cos \theta)(g_{nm} \cos m\varphi + h_{nm} \sin m\varphi) \times \{(n+1)(R_{\odot}/R)^{n+2} - n(R/R_s)^{n-1}c_n\}, \quad (1)$$

$$B_{\theta} = - \sum \frac{\partial P_n^m(\cos \theta)}{\partial \theta}(g_{nm} \cos m\varphi + h_{nm} \sin m\varphi) \times \{(R_{\odot}/R)^{n+2} + (R/R_s)^{n-1}c_n\}, \quad (2)$$

$$B_\varphi = - \sum \frac{m}{\sin \theta} P_n^m(\cos \theta) (h_{nm} \cos m\varphi - g_{nm} \sin m\varphi) \times \{ (R_\odot/R)^{n+2} + (R/R_s)^{n-1} c_n \}. \quad (3)$$

In these equations, $0 \leq m \leq n \leq N$ (in our case, $N = 9$), $c_n = -(R_\odot/R_s)^{n+2}$, P_n^m are the Legendre polynomials, g_{nm} and h_{nm} are the coefficients of the spherical harmonics calculated in the course of the solution of the boundary problem, θ is the co-latitude (counted from the poles to the equator) φ is the Carrington longitude, and R_s is the source surface radius. Usually it is assumed that $R_s = 2.5$. Hereinafter, the distances are measured in R_\odot and are counted from the center of the Sun.

In this work, we made use of a program that allowed us to calculate three components of the magnetic field in a spherical layer from the photosphere to the source surface Kharshiladze and Ivanov (1994). We performed summation over 10 harmonics and introduced a polar correction to make allowance for insufficient reliability of magnetic measurements near the poles Obridko and Shelting (1999). The coefficients of the expansion into spherical harmonics were found by the least square method without using the orthogonality of functions. The calculated magnetic field is limited to the latitudes $\pm 75^\circ$.

There are publications (see the discussion in Wang and Sheeley, 1992), which point out the shortcomings of the classical method and propose the hypothesis of radial magnetic field in the photosphere. Our calculations Obridko, Shelting, and Kharshiladze (2006) have shown that when these two methods are used, the differences do exist and concern mainly the intensity of the magnetic field. At the same time, the differences in the structure of the field lines are insignificant, especially over large time intervals. Therefore, it can be assumed that the rotation characteristics we find do not strongly depend on the method applied. A slight difference between the results obtained by these two methods are noticeable at latitudes higher than 70° .

3. The rotation period as a function of distance from the center of the Sun

To study the variation in the differential rotation of the solar corona with distance, the magnetic field was calculated at 14 selected distances from the base of the corona to the source surface. These are the heliocentric distances from $1.0 R_\odot$ to $2.2 R_\odot$ with a step of $0.1 R_\odot$ and a the distance of $2.45 R_\odot$. The distance of $1.0 R_\odot$ corresponds to the base of the corona and the distance of $2.45 R_\odot$, to the coronal layers in the vicinity of the source surface. We did not use the field on the source surface, where, in accordance with the boundary conditions, there only exists the radial field component. For each day in the period from 24 June 1976 to 31 December 2004, three field components were computed for the heliolatitudes from -75° to $+75^\circ$ with a step of 5° . Then, the total magnetic field B was calculated as the square root of the sum of squares of the three components.

After that, the method of periodogram analysis was applied. In this method, the correlation between the daily values of the calculated magnetic field and the test harmonic function with a trial period T_p is determined within the time window of a chosen length L . The correlation coefficient found shows the degree of similarity between the function with the period T_p and the distribution we are examining in this time window. After that, the window is shifted in time by Δt and the whole procedure repeats. The periodogram method ensures quite a good resolution in period, which allows a detailed study of the time–latitude characteristics of the coronal rotation.

In this work, periodograms were calculated with a window of 365 days (1 year) and a step of 3 solar rotations (81 days) for each series of the magnetic field data obtained. The total number of steps (windows) within the time interval mentioned above (24 June 1976 to 31 December 2004) was 125. The calculations were performed at each selected distance for the latitudes from 0° to $\pm 75^\circ$ with a step of 5° . The periods of the trial harmonic functions T_p varied from 22 to 36 days with a step of 0.1 day, *i.e.*, the total of 140 values.

The coronal rotation period T at a given distance and at a given specific latitude was determined as follows. At each latitude, we obtained a sequence of 125 time intervals (windows) for a given distance. Every such window contained 140 values of the periods of the trial harmonic functions with different amplitudes, characterizing the degree of similarity of the trial function to the initial distribution of the magnetic field intensity. At each step, we selected the oscillation period of the trial harmonic function with the maximum amplitude in the moving window. This means that the selected trial function had the maximum correlation (the greatest similarity) with the initial distribution we were examining in the given window. The period T_p found in such a way can be assumed closest to the “quasi-period” of the original observed distribution at this step. This period was taken as the synodic period of the coronal rotation T at a given time at a given latitude. Thus, we obtained the time dependence of the coronal rotation period at a given latitude (for examples see Badalyan and Sýkora, 2005, Badalyan and Sýkora, 2006, Badalyan, Obridko, and Sýkora, 2006, Badalyan, 2010). We called this procedure the method of maximum amplitudes.

Thus, we obtain a series of the coronal rotation periods at each latitude at different distances as a function of time. Every such series allows us to find the mean rotation period at a given latitude for the entire time interval under consideration and to study its time variations. At each distance, we have 31 such series. The totality of the series obtained for all heliocentric distances under consideration demonstrates how the coronal rotation changes with distance from the center of the Sun.

Figure 1 shows by way of example the maps (two-dimensional periodograms) for the distance $1.1 R_\odot$ and the latitudes 10° and 55° North. The color on the maps characterizes the height of amplitude for a given rotation period. One can see the selected periods form a kind of a broken band in the vicinity of a certain period characteristic of a given distance. We can observe the shift of this band on the maps that represent the mean synodic period of the corona *vs.* latitude (the differential rotation). In Figure 1, this shift is noticeable when passing from

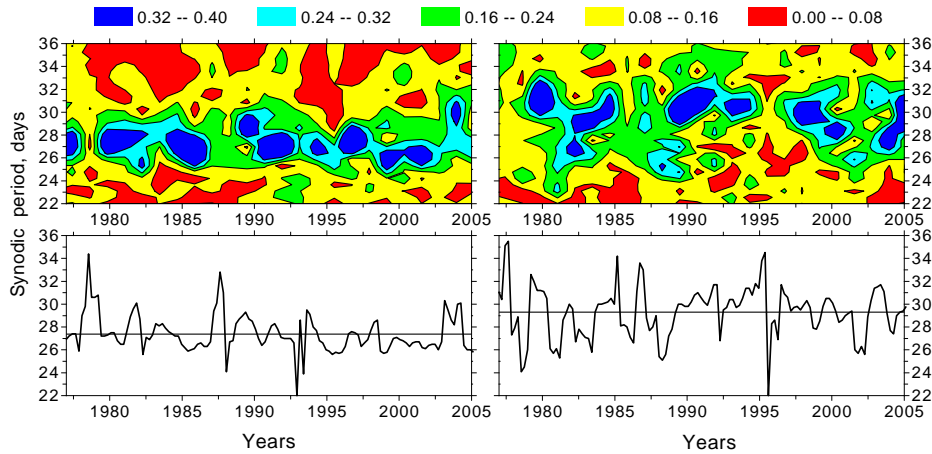


Figure 1. Two-dimensional periodograms for the latitudes of 10° (*left*) and 55° (*right*) North and the distance of $1.1 R_\odot$. The *lower panels* show the periods with maximum amplitudes in a moving time window.

the latitude of 10° higher, to the latitude of 55° . It is seen that, on average, the band shifts to longer periods.

The kinks of the band characterize the behavior of the rotation period with time. This is illustrated on the lower panels, under the maps. The plots represent the periods with maximum amplitudes at each step in the moving time window and illustrate the time variation in the coronal synodic period at the given latitude. The mean rotation period over the time interval under consideration is 27.4 days at the latitude of 10° and 29.3 days at the latitude 55° . These values are shown on the plots with straight horizontal lines.

Thus, the synodic rotation periods of the corona were determined at 14 distances from the center of the Sun for all latitudes in the time interval under examination. First, we found the mean period at every latitude from -75° to $+75^\circ$ (31 values), at each of the 14 distances. Figure 2 illustrates the mean latitude dependence of the synodic period for a few distances. Note that the curves in the figure are symmetric about the equator (the heliolatitude is zero). This means that the average periods for the northern and southern hemispheres were calculated for each latitude, and then, the approximating polynomial was drawn over the points obtained. In fact, at low latitudes there is a noticeable north–south asymmetry of rotation, which can be seen in some figures below.

Figure 2 reveals the following particularities of the relations obtained:

1. The differential gradient of the coronal rotation decreases with the heliospheric distance – as the distance increases, the curves become flatter.
2. The synodic period at the equator ($\varphi = 0$) increases gradually (the rotation rate decreases) with the increase of the distance.
3. Even in the vicinity of the source surface ($2.45 R_\odot$), the rotation of the corona remains differential.
4. Some decrease of the rotation period is observed at high latitudes at short heliocentric distances. This particularity was noted by Stenflo (1989). It can

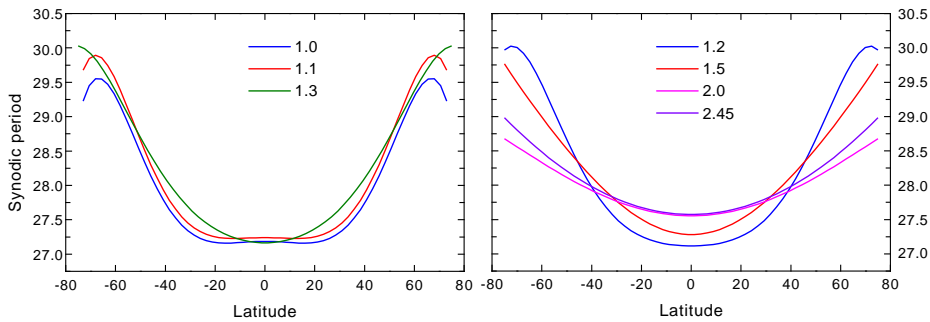


Figure 2. Synodic rotation period of the corona *vs.* latitude for some heliocentric distances indicated on the panels.

also be noticed when determining the rotation of the green-line corona (Letfus and Sýkora, 1982, Fig. 7).

The series of latitudinal dependencies of the rotation periods at various distances makes it possible to construct the general distribution of the corona rotation periods in the form of a map in the time–latitude coordinates. Figure 3 represents such maps for the distances of $1.1 R_{\odot}$ and $2.0 R_{\odot}$. The maps show that the rotation periods at both distances increase with latitude. For the convenience of comparison, the same scale was used for both maps. The bottom panel shows the monthly mean sunspot numbers in the new system (Version 2).

As seen from Figure 3, the rotation period increases with distance (the rotation rate decreases) throughout the map. At low latitudes, the periods on both maps do not exceed 28 days. However on the map for $2.0 R_{\odot}$, the total area of the regions where the rotation rate is maximum (*i.e.*, the period is less than 27 days, red color) is smaller than on the map for $1.1 R_{\odot}$. It is interesting to note that at $2.0 R_{\odot}$, the rapidly rotating regions are usually observed after the cycle maximum, at the beginning of the descending branch. In Cycle 23, which was lower than the other two cycles, the periods less than 27 days are virtually absent at $2.0 R_{\odot}$. At high latitudes, the maps do not display any visible periodicity in the appearance of slowly rotating regions (rotation periods more than 30 days, blue color), though there is a hint that they rather tend to form near the minimum of the cycle. Note also that on the map for $2.0 R_{\odot}$, such regions are significantly fewer and the general range of the periods is smaller than on the map for $1.1 R_{\odot}$. This agrees with Figure 2 (right panel), where the dependence on latitude for $2.0 R_{\odot}$ is flatter than for $1.1 R_{\odot}$ (left panel).

4. Rotation period *vs.* the phase of the activity cycle

To study the variations in the coronal rotation period during an activity cycle, we use the notion of the phase of the cycle. According to Mitchell (1929), the phase is determined as

$$\Phi = (\tau - m)/(|M - m|). \quad (4)$$

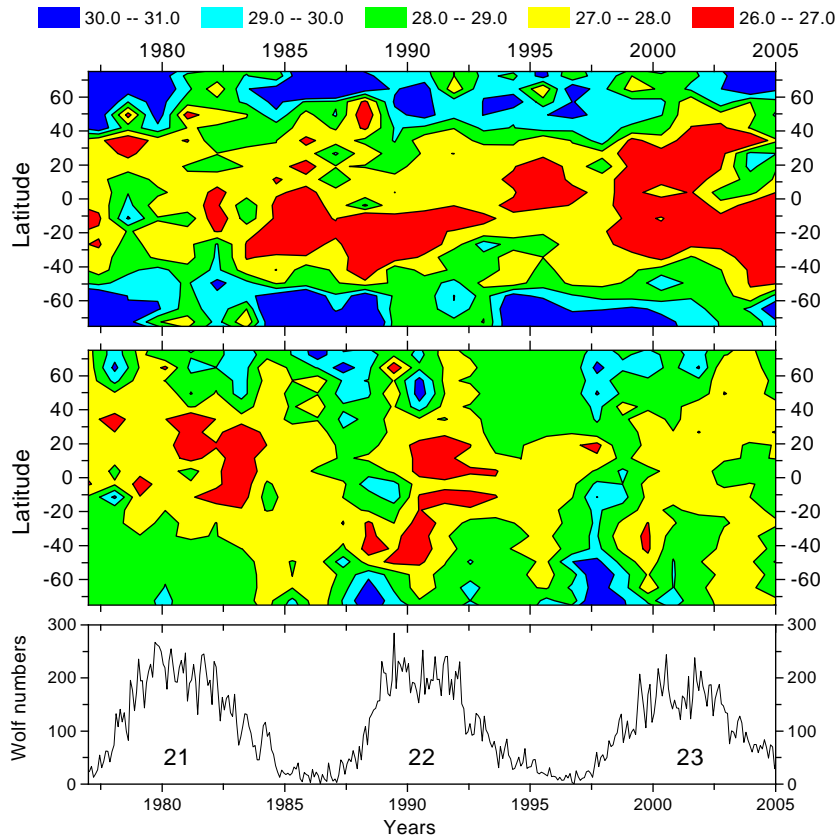


Figure 3. Time–latitude maps of the rotation periods for the distances $1.1 R_{\odot}$ (*top*) and $2.0 R_{\odot}$ (*middle*). The *lower panel* gives sunspot numbers in the new system (Version 2).

Here, τ is the current time, M and m are the times of the nearest maximum and minimum of the 11-year cycle, respectively. As follows from this definition, the phase is 0 at the minimum of each cycle and ± 1 at the maximum. The phase is positive on the ascending branch and negative on the descending branch of the activity cycle. The data for several activity cycles can be represented as a function of the phase of the cycle using the method of superposition of epochs under the assumption that the activity evolves by the same scenario in all cycles.

The maps in Figure 4 illustrate the distribution of the synodic periods of rotation of the coronal magnetic field at various distances from the center of the Sun plotted in the phase-latitude coordinates. The distributions refer to a certain mean activity cycle and are plotted as follows. The phase is determined at 125 time points for which the rotation periods were found earlier. Then, the periods are averaged over phase at a step 0.1. This yields 20 values in the phase range from -1 to $+1$. Depending on the phase, the number of the averaged periods ranges from 3 to 10. The difference is due to the facts that, first, the ascending branch contains fewer points than the descending one and, second, Cycle 23 in the time interval under consideration is incomplete.

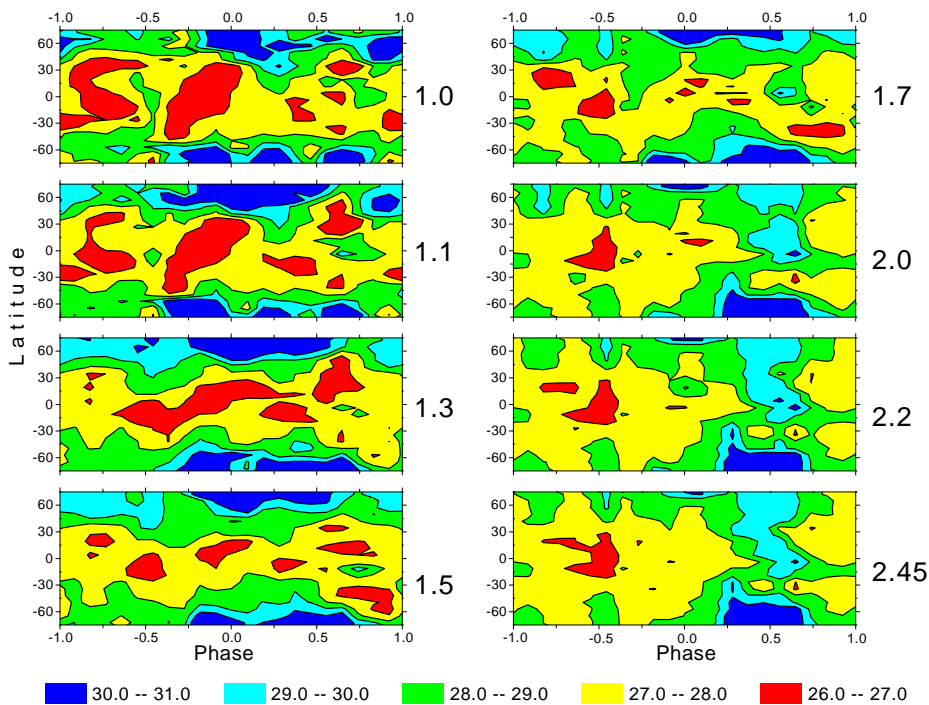


Figure 4. Distribution of the rotation periods of the solar corona on the phase–latitude maps calculated for various heliocentric distances in the range of $1.0 R_{\odot} - 2.45 R_{\odot}$. The distances in solar radii are indicated on the *right* of each map. The scale of the synodic rotation periods of the corona are given at the *bottom*.

The first thing that catches the eye is that the maps are similar up to the distance of $1.3 R_{\odot} - 1.4 R_{\odot}$. This particularly concerns the regions of relatively fast rotation observed in the descending branch until the minimum (periods of 26–27 days). As the distance increases, these regions disappear abruptly. The fast-rotating region splinters and after that its characteristic dimensions do not exceed 0.1 in phase. This may mean that such a particularity of the coronal rotation is most likely associated with large activity complexes that often appear in the descending branch. The characteristic size of the complexes is $30^{\circ} - 40^{\circ}$, *i.e.*, about 0.1 radius of the Sun. The contribution of the magnetic field of such objects to the general magnetic structure at $1.4 R_{\odot}$ decreases by at least an order of magnitude.

The regions of medium rotation rates (periods of ≈ 28 days), on the contrary, retain their structure in the equatorial zone up to $\approx 1.9 R_{\odot}$ independent of the phase of the cycle, and only at larger distances on the ascending branch of activity they are replaced by even lower rotation rates (longer periods).

And finally, the slowest rotation (colored blue on the maps) is observed in the polar zones at the minimum of activity and the beginning of the ascending branch. Note that the lifetime of these large periods somewhat differs in the two hemispheres, being much longer in the southern hemisphere.

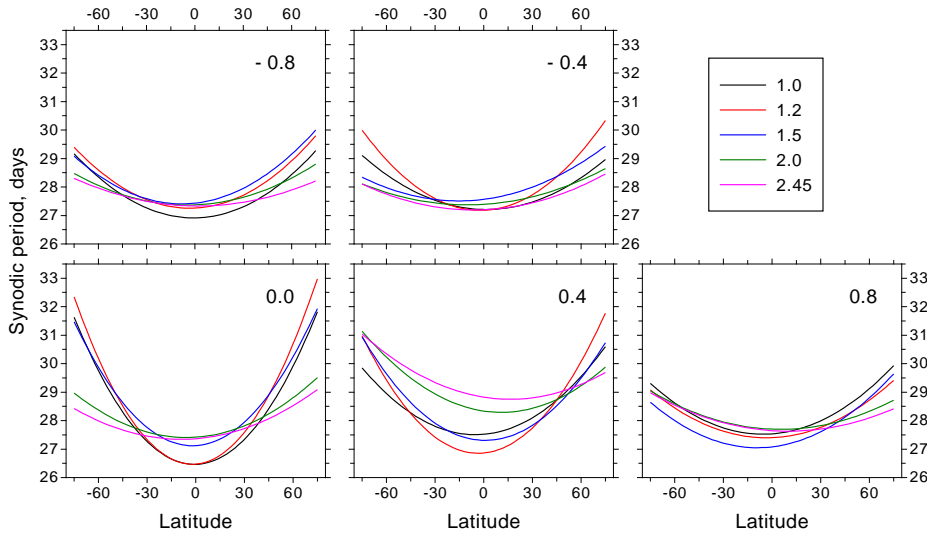


Figure 5. Synodic rotation periods of the corona as a function of latitude for different distances and phase intervals of the cycle. The mean phase values are indicated on the panels; the scale of distances in solar radii is given on the *right top panel*.

Now, consider the dependence of the coronal rotation on the phase of the activity cycle in more detail. For this purpose, we divided the phase interval from -1 to $+1$ into 5 sub-intervals of length 0.4, and averaged the rotation periods (from 18 to 40 values) within each sub-interval. Thus, for example, within the sub-interval centered at phase 0 (Figures 5–reff-fivemaps), the periods were averaged in the range of phases from -0.2 to $+0.2$. Then, the rotation period was plotted as a function of latitude for each of the five “phases” at all 14 distances under consideration.

Figure 5 illustrates the mean distributions of the rotation periods *vs.* latitude at five selected distances. The mean phase values are given on the panels. The scale on the right shows the color of the curve for a given distance. According to the definition Equation 4, phase $\Phi = -0.8$ corresponds to the beginning of the descending branch, $\Phi = -0.4$ is close to the middle of the descending branch, $\Phi = 0$ marks the minimum of the cycle, $\Phi = +0.4$ is close to the middle of the ascending branch, and $\Phi = +0.8$ is close to its end. A second-order polynomial was constructed using the points belonging to a given phase at a given height.

Figure 5 shows that the mean latitudinal dependencies are more or less steep parabolic curves (“plates” of different depth) for all phases. The curves for $\Phi = -0.8$ and $\Phi = +0.8$ are the flattest at all distances. This means that the rotation periods have similar values at all latitudes, *i.e.*, the differential gradient is small. The steepest (lowest) curves on the lower left-hand panel for distances not exceeding $1.5 R_{\odot}$ refer to the minimum of the cycle; in other words, at the minimum, the coronal rotation period changes most abruptly (the differential gradient is the largest) when passing from the equator to higher latitudes. The highest curve (largest rotation periods; *i.e.*, smallest rotation rates) refers to phase $+0.4$, which is close to the middle of the ascending branch. This agrees

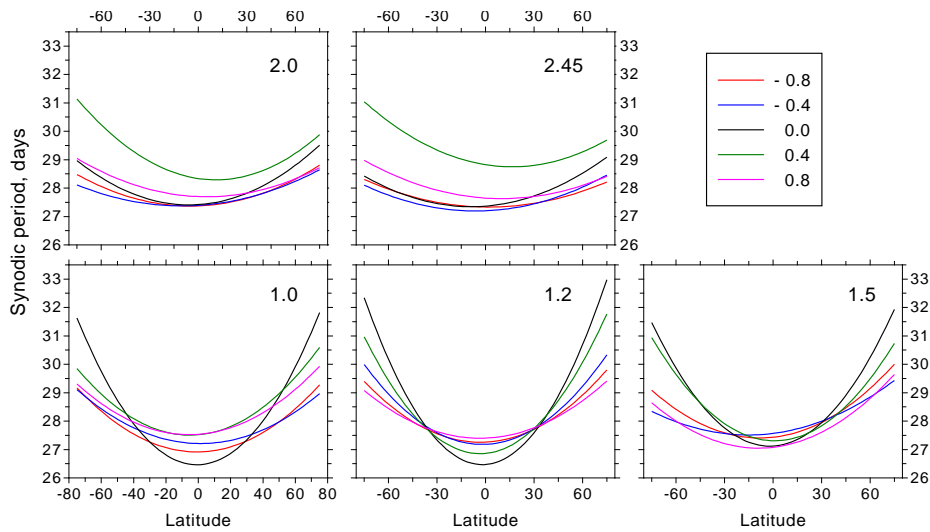


Figure 6. The profile of the curves in relation to distance in different phase intervals. The distance in solar radii is given on the panels; the phase scale is provided on the *right-hand top panel*.

with the distribution of the periods in Figure 4 for large distances, where a broad vertical band of large periods is seen in the middle of the rise phase.

Figure 6 compares the profile of the curves for the same phase intervals at different distances. At small distances (lower panels) the steepest curves refer to the minimum of the cycle. The closer we are to the maximum both along the ascending and along the descending branch, the flatter become the curves. At large distances (upper panels), all curves are rather flat. Here, the highest curves (largest periods) at both distances refer to phase $\Phi = +0.4$, *i.e.*, to approximately the middle of the ascending branch of the activity cycle. At this time, the rotation of the corona at large distances is the slowest, and the differential gradient (the change of the rotation period with heliolatitude) is small.

The general distribution of the corona rotation periods with the distance for five phase intervals during a cycle is represented in more detail in Figure 7. Each cycle is divided into five intervals so that the duration of each interval is about two years. Figure 7 shows that the field distributions differ in different phases, the maps changing asymmetrically with respect to the activity minimum. For example, the map for $\Phi = -0.4$ differs essentially from that for $\Phi = +0.4$. The maps for $\Phi = -0.8$ and $\Phi = +0.8$ demonstrate a pronounced north–south asymmetry in the distribution of the rotation periods: on the former, one can isolate a band of fast rotation (small periods) at latitudes of about 20° North, while on the latter, such a band is absent, but there are two bands of fast rotation more or less symmetric about the equator that do not go beyond $2 R_\odot$. At the minimum, the N–S asymmetry is not observed. The band of fast rotation is located at equatorial latitudes and goes from the base of the corona up to the source surface. While moving to higher latitudes at the minimum of the cycle, the periods increase significantly; the differential gradient on the map is the largest.

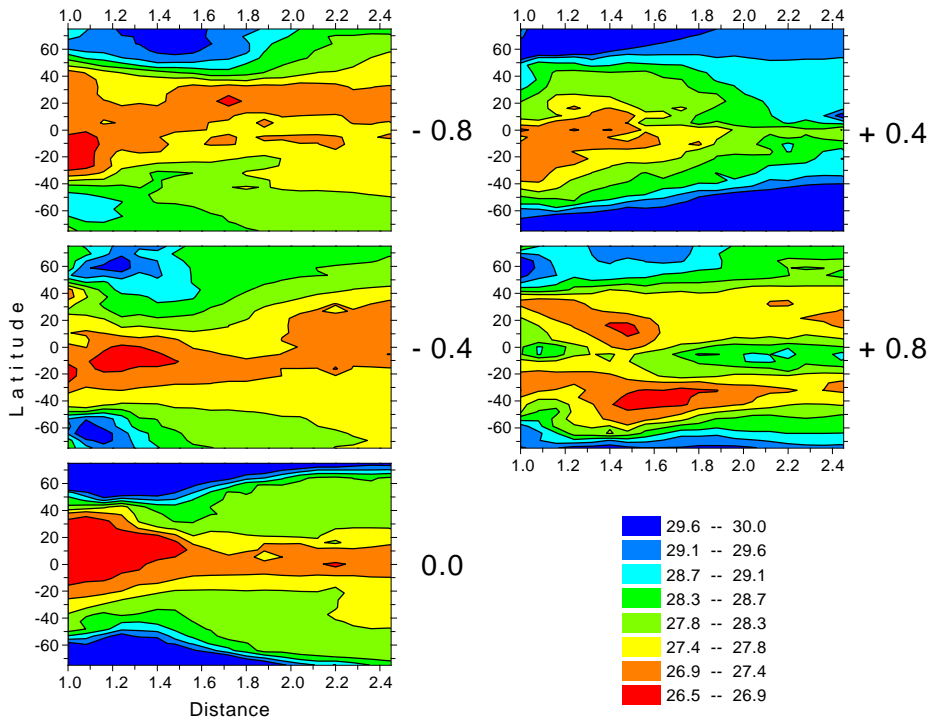


Figure 7. Rotation periods in the distance–latitude reference frame. The cycle phases are given on the *right* of the maps.

Immediately after the maximum at the beginning of the descending branch (left highest panel), the zone of small rotation periods at short distances ($< 1.5 R_{\odot}$) is located near the equator. At the same time, the zone of moderate rotation rates (periods of 26.9–27.4 days), which exists throughout the descending branch including the minimum (left lowest panel), extends to large heights. During the entire descending branch, a zone of small rotation rates (periods of 29.6–30.0 days), forms gradually at high latitudes. Immediately after the maximum, this zone is only seen in the north hemisphere at relatively small heights (left highest panel), but at the end of the descending branch (left lowest panel) and particularly, at the beginning of the ascending branch (right highest panel), it extends to all heights in both hemispheres. By this moment, the zones of moderate rotation rates at large heights disappear, being only observed up to the height of $1.6 R_{\odot}$. In the equatorial region, the smallest periods are not observed at all. As the maximum of the cycle approaches, the velocity field at mid latitudes is restored and the zones of large periods at the poles decrease.

5. Characteristics of differential rotation of the corona at different distances

To obtain the parameters of differential rotation and consider its cycle variation, we used the traditional Faye formula:

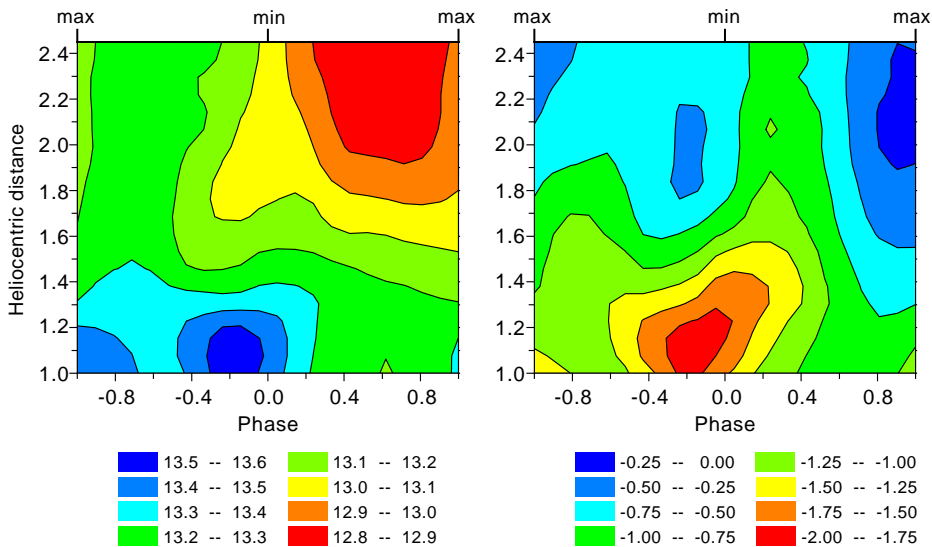


Figure 8. The phase–latitude distribution of a (left) and b (right). The scale at the bottom provides the coefficients in degrees per day.

$$\omega = a + b \sin^2 \varphi. \quad (5)$$

Here ω is the angular synodic rotation rate in degrees per day; a is the coefficient that characterizes with some approximation the angular rotation rate of the Sun near the equator; and b is the change in the rotation rate with latitude. For the Sun, the latter coefficient is negative; *i.e.*, the rotation rate decreases (period increases) with latitude. Coefficient b is often called the differential gradient. In the general case, a and b depend on the height of the object under examination (*e.g.*, coronal magnetic field) in the solar atmosphere and on its variation with the phase of the cycle.

To compute a and b , the data for all latitudes in each of the five phase intervals were combined in a single series and the periods were converted to synodic angular velocity. Each series contains 31 points at a given distance. They were used to determine a and b from the slope of the $\omega = f(\sin^2 \varphi)$ line. Computations were carried out up to latitudes 60° inclusive. At higher latitudes, the Faye law requires that the fourth degree of the sine of latitude be included. The diagrams of the phase–latitude distribution of a and b are represented in Figure 8.

Figure 8 shows that coefficient a (left panel) in the time interval under consideration is the largest near the cycle minimum, where its value reaches 13.6° per day (*i.e.*, the synodic period is 26.4 days).

Note that analyzing daily Doppler measurements for the period 1967–1976, R. Howard arrived at the conclusion that a reached its maximum exactly at the cycle minimum in 1976 Howard (1976). The relation obtained by Howard is close to a similar relation for sunspots. In a later work Howard, Gilman, and Gilman (1984), the authors analyzed dependencies for the rotation characteristics of

individual sunspots inside a group. It turned out that the equatorial rotation rate decreases with the increase of the spot area. The equatorial rotation rate increases noticeably in the vicinity of the cycle minimum, while the differential gradient decreases abruptly 1-2 years before the minimum. In Belvedere *et al.* (1977), the authors make even a more general conclusion that at all levels in the solar atmosphere, the objects with smaller sizes and shorter lifetimes rotate faster than large-scale and long-lived objects.

Such a high equatorial rotation rate is only observed at the minimum of the cycle at distances no more than $1.4 R_{\odot}$. The smallest coefficient a on the map (*i.e.*, the lowest rotation rate) is seen at large distances at the middle of the ascending branch. One can also see a horizontal band (zone) at a distance $\sim 1.5 - 1.6 R_{\odot}$, in which a does not virtually change and is approximately 13.2° per day in all phases of the cycle. It is interesting to note that this velocity corresponds to the Carrington period of 27.2753 days the Carrington reference frame $360/27.2753 = 13.19875$.

The right-hand panel of Figure 8 shows that the negative coefficient b has the largest absolute value at small distances near the cycle minimum approximately where the largest values of a are observed. At larger distances, b is small. The differential gradient here is small, the rotation rate almost does not change with latitude. On the same panel, we can also see a band of relatively increased values of coefficient b (slightly increased differential gradient) in the middle of the ascending branch of activity. This band exists at all distances and the differential gradient somewhat decreases with distance.

6. Comparison with the corona rotation as inferred from green-line observations

The differential rotation of the solar corona inferred from the coronal green-line brightness was studied by many authors (for some references, see Introduction). We have examined this issue in detail in Badalyan and Sýkora (2005, 2006); Badalyan, Obridko, and Sýkora (2006); Badalyan (2010). The studies were carried out using the database by J. Sýkora (Slovak Republic). J. Sýkora was the first to take over a difficult task of reducing observational data from different coronal stations to a single photometric system. The discussion of the arising problems and the first results were published in 1971 Sýkora (1971b). As the amount of data was increasing, the work was continued (Sýkora, 1980, 1992, 1994, Storini and Sýkora, 1997, Sýkora and Rybák, 2005).

The database contains the results of measurements of the brightness of the coronal green line reduced to a single photometric scale with a step of 5° in latitude and $\approx 13^{\circ}$ in longitude (1 day). It covers the interval 1939-2001. During the first few years, the observations were irregular, therefore the data are mainly used since 1943. Original daily measurements taken separately on the eastern and western limb were used to derive brightness on the central meridian on each particular day. It was obtained as the mean of the values measured on the eastern limb 7 days before a given date and on the western limb 7 days after it (*i.e.*, approximately at the moments when a meridian corresponding to the central

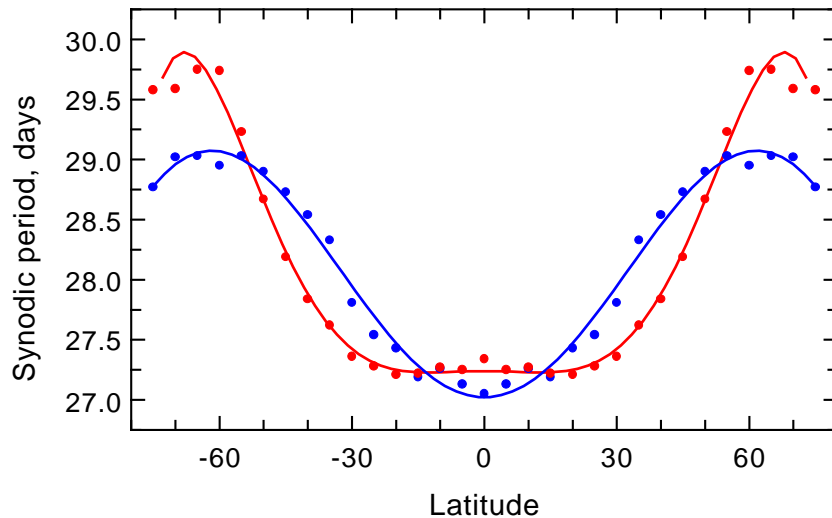


Figure 9. Synodic periods of the differential rotation of the solar corona as determined from the green-line brightness (*blue curve*) and magnetic-field data at the distance $1.1 R_{\odot}$ (*red curve*).

meridian on the given day was passing through the eastern and the western limb, respectively). The green-line brightness is adjusted to the height of $60''$ above the limb (the height of Pic-du-Midi measurements Trellis (1957)). This is close to the distance of $1.1 R_{\odot}$ from the center of the disk.

Latitudinal variations in the synodic periods of the coronal differential rotation determined from the data on the green-line brightness (blue curve) and magnetic field at $1.1 R_{\odot}$ (red curve) are compared in Figure 9. As in Figure 2, the curves are symmetric with respect to line $X = 0$ (with respect to the equator); *i.e.*, the data for the northern and southern hemispheres are averaged. The green-line curve covers the period 1943-2001; the magnetic-field curve, the period 1976-2004.

As follows from Figure 9, both the green-line brightness and the magnetic field data confidently reveal the differential rotation of the corona. At the same time, there are noticeable differences between the two curves. The green-line curve is mainly located inside the curve of the magnetic field and displays smaller gradient to higher latitudes. The magnetic-field curve shows that short periods persist without significant change up to the latitudes of $30^{\circ} - 35^{\circ}$. As the latitude increases further, a sharp increase in the rotation period occurs, and at the highest latitudes, the magnetic field shows a lower rotation rate than the green-line brightness.

Figure 10 represents the maps of distribution of the corona rotation periods derived from the green-line (top) and magnetic-field (bottom) data in the phase-latitude coordinates. The figure reveals the similar and different features on the two maps. Thus, the low-latitude band of high rotation rates (periods less than 28 days) occupies approximately the same latitude range. There is also some similarity in the distribution of the fastest rotation rates (periods less than 27 days). At higher latitudes, one can see the zones of slower rotation, but their

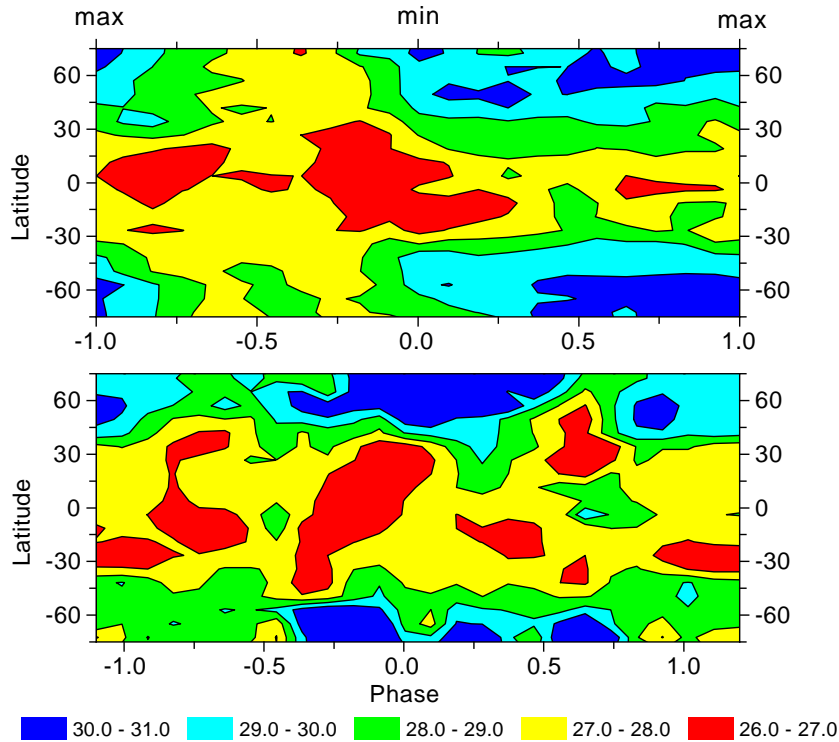


Figure 10. Cycle distribution of the rotation periods based on the green-line (*top*) and magnetic-field (*bottom*) data.

location on the maps is different. The map based on the green-line brightness shows that, in the middle of the descending branch of activity, the rotation rates at high latitudes are close to those at low latitudes (the band of small differential gradients at $\Phi \approx -0.5$). The zones of slow rotation arise at the middle of the ascending branch and extend partly to the maximum. These particularities of rotation inferred from the green-line data were considered in detail in Badalyan, Obridko, and Sýkora (2006); Badalyan (2009, 2010). On magnetic maps, the zones of slow rotation at high latitudes are mainly observed in other phases of the cycle and become dominant near the cycle minimum.

Let us compare the differential rotation curves for five selected phase intervals. Figure 11 is an analog of Figure 5 for the green-line brightness (left) and magnetic field (right). When considering the figure, one can readily notice the difference in the depth of the approximating curves on the left (green line) and right (magnetic field) panels. The curves on the left panel are flatter than the curves on the right panel. This means that magnetic data suggest stronger differential gradient of rotation than the brightness of the coronal green line. The flattest curve is the curve for $\Phi = -0.4$ on the left panel (middle of the declining phase). This agrees with the band in the left-hand part of the upper map in Figure 10. In this phase, the green corona displays the smallest differential gradient. The steepest curve

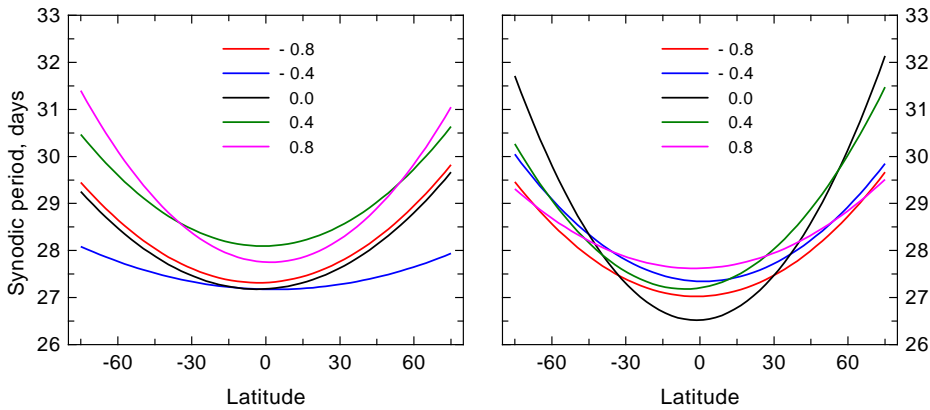


Figure 11. Dependence on the phase of the cycle for the differential curves based on green-line data (*left*) The same for the curves based on magnetic data at the distance of $1.1 R_{\odot}$ (*right*). One can see that the curves themselves as well as their cycle variations are different.

in Figure 11 is the parabola for $\Phi = 0$ on the right panel (magnetic data). The same effect is seen on the lower map in Figure 10 at the minimum of the cycle.

Thus, as expected, there isn't and cannot be complete correspondence between the rotation characteristics determined by the green line and by the magnetic field. It is well known that the green-line emission depends on the temperature and density of plasma. The problem of the corona heating has been considered by many authors (see references in Mandrini, Démoulin, and Klimchuk, 2000, Badalyan and Obridko, 2007). All heating mechanisms existing nowadays depend in different ways on the strength and spatial dimensions of the magnetic field. The relative contribution of these mechanisms varies depending on the latitude and the phase of the solar cycle. Nevertheless, there is a certain similarity between the rotation characteristics, which may be an additional argument in favor of the applicability of the proposed method.

7. Conclusion

In this paper, we have considered the possibility of using magnetic data to study the rotation of the solar corona. Magnetic field controls the structure of coronal objects. Therefore when studying the differential rotation of the magnetic field, we actually use the latter as tracers to analyze variations in the rotation parameters with distance and with the phase of the activity cycle. The coronal magnetic field is calculated by extrapolating the fields observed in the photosphere. Thus, the method proposed in our work makes it possible to study the characteristics of differential rotation of the corona in a wide range of heights and in different phases of the cycles.

Our study covers the time interval from 24 June 1976 to 31 December 2004; *i.e.*, Cycles 21, 22, and part of Cycle 23. It is shown that the differential gradient (the range of rotation rate variations with latitude) decreases with distance from the center of the Sun. The rotation rate at the equator decreases gradually (*i.e.*,

the rotation period increases) with the increase of the distance. However the rotation remains differential even at the source surface, that is at about $2.5 R_{\odot}$ from the center. The latter is very important for calculating the spatial structure of the solar wind and possible changes in the sector structure when moving away from the ecliptic plane.

Variations in the differential rotation of the corona with the phase of activity cycle have been considered in detail. In the time interval under consideration, the largest differential gradient is detected at short distances (no more than $1.4 R_{\odot}$) from the center in the equatorial zone. Both at the ascending and at the descending branch of activity, the rotation of the corona is the less differential the closer we are to the maximum of activity. At the same time, the rotation parameters in the phases symmetric with respect to the cycle minimum are different. Besides that, the north–south asymmetry of rotation noticeable in other phases of the cycle is not observed at the minimum.

The time interval selected for examination allowed us to compare the rotation parameters obtained by our method based on magnetic data with the parameters obtained earlier in the photosphere from observations of various tracers and in the corona from observations of the green-line brightness at low altitudes. The results show a satisfactory agreement, though one can also notice some differences.

Our results show that when going to higher coronal levels, the essentially differential rotation is becoming increasingly rigid. As follows from the calculation procedure itself, this is accompanied by disappearance of high-order harmonics. The energy contribution of different harmonics depends on distance as a power-law function with exponent $\beta = -2(n + 2)$, see Equations 1– 3. Thus, as the heliocentric distance increases, we encounter objects of increasingly large scales. Besides, non-radial components disappear more rapidly, and at $2.5 R_{\odot}$ the field becomes strictly radial.

This reminds us of the change in the rotation characteristics with depth in the subphotospheric layers. There is certainly a great difference between the basic processes in the corona and in the subphotospheric layers. The magnetic field is not generated in a stationary solar corona, which allows us to use the potential approximation in our calculations. The calculated magnetic field in the corona is completely determined by the conditions in the photosphere and subphotospheric layers. In up-to-date models, the characteristic spatial scales of the magnetic fields depend on their generation region. The fields of higher scales are generated deeper under the photosphere. So, the rotation characteristics of the corona can reflect variations in the plasma rotation rate under the photosphere. Thus, according to modern concepts, the coronal rotation reflects the rotation of the subphotospheric layers (*e.g.*, see Kitchatinov, 2013). The higher layers of the corona reflect the rotation of the deeper layers of the Sun. The proposed method allows us to expect that the study of the corona rotation at distances from its base up to the source surface will make it possible to “look” into the subphotospheric layers and calculate the rotation parameters therein. The results obtained in this work suggest that either the generation depth of magnetic fields of different scales or the generation process itself and its amplitude change during an activity cycle. In future, we are going to apply the results obtained to the study of rotation of deep sub-photospheric layers of the Sun.

8. Acknowledgements

The work was supported by the Russian Foundation for Basic Research, Project 17-02-00300. We are grateful to the WSO team for the data available on the Internet site WSO.stanford.edu/forms/prsyn.html.

Disclosure of Potential Conflicts of Interest The authors declare that they have no conflicts of interest.

References

- Altrock R.C.: 2003, *Solar Phys.*, **213**, 23. DOI. ADS.
- Antonucci, E., Svalgaard, L.: 1974, *Solar Phys.*, **34**, 3. DOI. ADS.
- Badalyan, O.G.: 2009, *Astron. Zh.*, **86**, 295 (English translation 2009, *Astron. Reports*, **53**, 262). DOI. ADS.
- Badalyan, O.G.: 2010, *New Astron.*, **15**, 135. DOI. ADS.
- Badalyan, O.G., Obridko, V.N.: 2007, *Pis'ma Astron. Zh.*, **33**, 210 (English translation 2007, *Astron. Lett.*, **33**, 158). DOI. ADS.
- Badalyan, O.G., Obridko, V.N.: in Stepanov, A.V. and Nagovitsyn, Yu.A. (eds.), *Solar and solar-terrestrial physics 2015*, St.-Petersburg, Astron. Obs. RAS at Pulkovo, 13 (in Russian), http://www.gaoran.ru/russian/publ-s/conf-s/conf_2015/conf_2015.pdf.
- Badalyan, O.G., Sýkora, J.: 2005, *Contrib. Astron. Obs. Skalnaté Pleso*, **35**, 180. ADS.
- Badalyan, O.G., Sýkora, J.: 2006, *Adv. Space Res.*, **38**, 906. DOI. ADS.
- Badalyan, O.G., Obridko, V.N., Sýkora, J.: 2006, *Astron. Zh.*, **83**, 352, (English translation 2006, *Astron. Reports*, **50**, 312). DOI. ADS.
- Belvedere, G., Godoli, G., Motta, S., Paterno, L., Zappala, R.A.: 1977, *Astrophys. J. Lett.*, **214**, L91. DOI. ADS.
- Brajša, R., Ruždjak, D., Vršnak, B., Pohjolainen, S., Urpo, S., Scholl, A., Wöhl, H.: 1997, *Solar Phys.*, **171**, 1. DOI. ADS.
- Hoeksema, J.T.: 1991, *Solar magnetic fields – 1985 through 1990*, Report CSSA-ASTRO-91-01.
- Hoeksema, J.T., Scherrer, P.H.: 1986, *The Solar Magnetic Field – 1976 through 1985*, WDCA Report UAG-94, NGDC, Boulder. ADS.
- Howard, R.: 1976, *Astrophys. J. Lett.*, **210**, L159. DOI. ADS.
- Howard R., Gilman P.I., Gilman P.A.: 1984, *Astrophys. J.*, **283**, 373. DOI. ADS.
- Insley, J.E., Moore, V.I., Harrison, R.A.: 1995, *Solar Phys.*, **160**, 1. DOI. ADS.
- Jurdana-Šepić, R., Brajša, R., Wöhl, H., Hanslmeier, A., Poljančič, L., Svalgaard, L., Gissot, S.F.: 2011, *Astron. Astrophys.*, **534**, A17. DOI. ADS.
- Kharshiladze, A.P., Ivanov, K.G.: 1994, *Geomagnetizm i Aeronomia*, **34**(4), 22 (in Russian). ADS.
- Kitchatinov, L.L.: 2013, *Solar and Astrophysical Dynamos and Magnetic Activity*, Proc. IAU Symposium, **294**, 399. DOI. ADS.
- Letfus, V., Sýkora, J.: 1982, *Atlas of the Green Corona Synoptic Charts for the Period 1947-1976*, Veda Publ. House, Bratislava. ADS.
- Makarov, V.I., Tlatov, A.G.: 1997, *Astron. Zh.*, **74**, 615. (English translation 1997, *Astron. Rep.*, **41**, 543). ADS.
- Mandrini, C.H., Démoulin, J., Klimchuk, A.: 2000, *Astrophys. J.*, **530**, 999. DOI. ADS.
- Mitchell S.A.: 1929, *Handb. Astrophys.*, **4**, 231.
- Mouradian, Z., Bocchia, R., Botton, C.: 2002, *Astron. Astrophys.*, **394**, 1103. DOI. ADS.
- Nash, A.G., Sheeley, N.R. Jr., Wang, Y.-M.: 1988, *Solar Phys.*, **117**, 359. DOI. ADS.
- Obridko V.N., Shelting B.D.: *Solar Phys.*, **184**, 187. DOI. ADS.
- Obridko, V.N.; Shelting, B.D.; Kharshiladze, A.F.: 2006, *Geomagnetizm i Aeronomia*, **46**, 294 (English translation 2006, *Geomagnetism and Aeronomy*, **46**, 294). DOI. ADS.
- Rybák, J.: 1994, *Solar Phys.*, **152**, 161. DOI. ADS.
- Rybák, J.: 2000, *Hvar Obs. Bull.*, **24**, 135. ADS.
- Sime D.G., Fisher R.R., Altrock R.C.: 1989, *Astrophys. J.*, **336**, 454. DOI. ADS.
- Stenflo, J.: 1989, *Astron. Astrophys.*, **210**, 403. ADS.
- Storini, M., Sýkora, J.: 1997, *Nuovo Cimento*, **20C**, 923. ADS.
- Sýkora, J.: 1971a, *Solar Phys.*, **18**, 72. DOI. ADS.

- Sýkora, J.: 1971b, *Bull. Astron. Inst. Czechosl.*, **22**, 12. ADS.
- Sýkora, J.: 1980, in Dryer, M. and Tandberg-Hanssen, E. (eds.), *Solar and Interplanetary Dynamics*, Reidel, Dordrecht, 87. ADS.
- Sýkora, J.: 1992, *Contrib. Astron. Obs. Skalnaté Pleso*, **22**, 55. ADS.
- Sýkora, J.: 1994, *Adv. Space Res.*, **14(4)**, 73. DOI. ADS.
- Sýkora, J., Rybák, J.: 2005, *Adv. Space Res.*, **35**, 393. DOI. ADS.
- Tlatov, A.G.: 1997, *Astron. Zh.*, **74**, 621. (English translation 1997, *Astron. Reports*, **41**, 548). ADS.
- Trellis, M.: 1957. *Ann. d'Astrophys.*, Suppl. No. 5. ADS.
- Wang, Y.M., Sheeley, N.R.: 1992, *Astrophys. J.*, **392**, 310. DOI. ADS.
- Zaatri, A., Wöhl, H., Roth, M., Corbard, T., Brajša, R.: 2009, *Astron. Astrophys.*, **504**, 589. DOI. ADS.